DYNAMICS OF A HIGH ALTITUDE LONG ENDURANCE UAV

Zdobyslaw Goraj
Warsaw University of Technology, Warsaw, Poland (goraj@meil.pw.edu.pl.)

Keywords: *stability, panel methods, airplane design*

Abstract

This paper presents dynamic analysis of a high altitude long endurance unmanned aerial vehicle (HARVE-2). Panel method has been used to compute aerodynamic characteristics of high wing monoplane with V-shape empennage. Weight prediction, finding mass distribution and computing the moments of inertia has been included into analysis. Steady trimmed flight conditions were found from a nonlinear set of equations of motion. Stability derivatives were computed basing on pressure distribution and were compared to those obtained from simplified engineering procedures. Damping and frequency coefficients for natural modes of vibrations were computed and discussed in details. A number of stability characteristics for various flight altitude and mass of the airplane (changeable with flight path) has been included and discussed in the paper. This analysis can be treated as a starting point for further refinement of dynamic characteristics in the context of flying and handling qualities.

1 Introduction

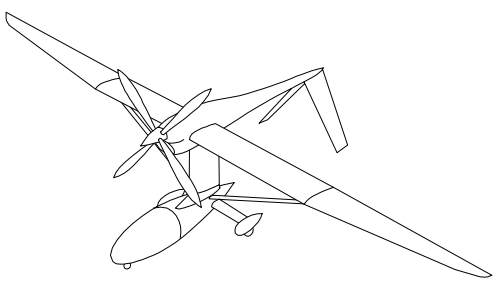

Fig.1 HALE UAV conceptual design

Stratospheric flights can provide wide, new opportunities for commercial, scientific and military activity. The reason to fly at ultra high altitudes is not only to see further at wider angle, but also to be safer against manned interceptor aircraft and also to fly above most commercial aircraft. Although powered airplanes have reached ultra high altitudes (more than 20 km) and they are able to operate continuously through long time (several days) there are still such areas of flight envelope where challenges of high altitude and long endurance (HALE) have not yet been met. Such aircraft must be unmanned and has to be operated autonomously or under remote control. Numerous UAV programs (including HALE missions designs) ended without becoming practical. It seems that there exist at least four serious obstacles, to overcome them can mean the successful building of HALE aircraft. These obstacles are very special aerodynamic (low Reynolds Numbers together with transonic speeds), very light structures usually of high aspect ratio, propulsion technology and flight control system (usually combining the best features of preprogrammed and hand-flown modes). Various conceptual projects of HALE UAV were presented and discussed by the author in the Aircraft Design Journal [1]. This paper focuses mainly on the flight dynamics and flight control system of the HALE UAV, selected among other configuration. It is a high-wing monoplane having 3600 kg starting mass, 26 km ceiling, 27000 km range and 54 h endurance. Analysis is based on the linearized equation of motion of a rigid aeroplane with deflectable elevator and ailerons. An important point in the analysis was estimating the stability

derivatives. Some of these derivatives change versus altitude due to change of viscosity and the boundary layer thickness. It was the reason that the stability derivatives were computed by means of modified panel methods, and compared with the results of classical engineering approach. Panel methods gave the estimation of the longitudinal and lateral stability derivatives of this complex configuration with a greater degree of confidence than could usually be ascribed to estimates of these derivatives by engineering methods (DATCOM [2] or ESDU [3]). The stability and control characteristics of the basic airplane were assessed in the context of flying and handling qualities requirements.

2 Design layout

To meet important requirements laid down in the high altitude long endurance patrol mission specification, a number of design configuration have been considered [4,5]. In this paper only a high wing monoplane will be considered because just this configuration has the best both specific range and endurance computed for the maximum endurance flight conditions [1]. Also, this configuration has the highest rate of climb and the shortest time to reach service ceiling. Wing has high aspect ratio equal to 19.3, span of 34 m and wing area equal to 60 m^2. Wing is supported to the main container by the double-rod angle strut, increasing both bending and torsional wing stiffness, Fig.2,3,4. Tailplane has V-shape of negative dihedral angle with full span and 25 % flaps chord. Three-point fixed landing gear is attached to the container. The fuselage is fixed with container using vertical thin-walled pylon. Sufficient power at departure altitude could be obtained only by the use of multistage turbocharger with a liquid intercooler. The compound propulsion system concept, developed by GROB Luft und Raumfahrt for STRATO 2C, has been adopted, as a basic solution with a modification presented in [1]. The power requirement of the aircraft - a product of drag and airspeed - increases rapidly with altitude. A suitable regulated turbocharger of the modified, compound propulsion system can maintain its available power of 400 kW at a constant value right up to the design altitude. Details of the compound propulsion system are given in [1,4,5,6]. The construction of the aircraft is based on glass fibre / carbon fibre design, including the fuselage, the container with measuring apparatus and a spring undercarriage [7].

3 Masses and moments of inertia

The most important airplane components with their mass values (kg) and coordinates of mass centres (m.) are given in Tab.1 All coordinates are given in the design frame of reference, fixed to the quarter of Mean Aerodynamic Chord (MAC). Axis x is parallel to MAC and is directed backwards of airplane, axis z is perpendicular to x axis and directed upwards.

Tab.1 Airplane components, their masses and coordinates

N	Airplane components	mass	x	y	z
1	right wing	256	0.5	15	0
2	left wing	256	0.5	-15	0
3	fore body	11.4	-2	0	0
4	main body	114	0	0	0
5	rear body	126	2.5	0	0
6	right tailplane	46	6.3	2.4	-1.5
7	left tailplane	46	6.3	-2.4	-1.5
8	right strut	25	0	2.9	-1.7
9	left strut	25	0	-2.9	-1.7
10	power unit	250	-1.5	0	0
11	pylon	22	0.4	0	-1.7
12	container	86	-0.5	0	-3.5
13	apparatus	300	-1	0	-3.5
14	front wheel	20	-1.5	0.	-4.5
15	right landing gear	30	2.4	2.5	-4.4
16	left landing gear	30	2.4	-2.5	-4.4
17	fuel I - right wing	750	0.69	5	0
18	fuel I - left wing	750	0.69	-5	0
19	fuel II- right wing	250	-0.3	8	0
20	fuel II- left wing	250	-0.3	-8	0

Mass of the whole airplane and its coordinates (in the variant with full fuel tanks) are equal to 3640 kg and (0.39 m; 0; -0.54 m), respectively. Coordinates of the pseudo-tensor of inertia are: Jx=219000 kg*m^2; Jy=14600 kg*m^2; Jz=220000 kg*m^2; JXZ=277 kg*m^2. In the case of empty main fuel tanks the whole airplane mass and its coordinates are equal to 2140 kg and (0.18 m; 0; -0.92 m), respectively.

4 Aerodynamic characteristics

In this paper all design decisions and recommendations were based on results obtained from panel method for thick surfaces. Panel method originates from Laplace's equation, $\Delta\Phi = 0$, for the velocity potential Φ and disturbance velocity potential φ [8,9]. The solution of Laplace's equation for the full velocity potential has the following form:

$$\Phi(x,y,z) = \frac{1}{4\pi}\int_{body+wake}\mu\frac{\partial}{\partial n}\left(\frac{1}{r}\right)dS - \frac{1}{4\pi}\int_{body}\sigma\frac{1}{r}dS + \Phi_\infty \quad (1)$$

The boundary conditions are as follows:

- inner Dirichlet's condition on the surface of the body

$$\frac{1}{4\pi}\int_{body+wake}\mu\frac{\partial}{\partial n}\left(\frac{1}{r}\right)dS - \frac{1}{4\pi}\int_{body}\sigma\frac{1}{r}dS = 0\,, \quad (2)$$

where

doublet strength: $\mu = -(\Phi - \Phi_i)$; (3)

source strength: $\sigma = \partial\mu/\partial n$. (4)

- Kutta-Zhukovsky condition at the trailing edge:

$$\Delta p(x,y)_{TE} = 0 \quad , \quad (5)$$

- condition on the wake:

$$\frac{\partial\varphi(x,y)}{\partial x} = 0 \ . \quad (6)$$

Assuming that the inner velocity potential Φ_i is equal to the potential at infinity, Φ_∞, then from eq. (1) one can obtain an integral equation in the form of equation (2). Eq. (2) can be approximated by a set of linear equations with unknown strength of doublets μ (being constant over each panel):

$$\sum_{k=1}^{N} C_k\mu_k + \sum_{l=1}^{N_w} C_l\mu_l + \sum_{k=1}^{N} B_k\sigma_k = 0, \quad (7)$$

where C_k, C_l i B_k are aerodynamic influence coefficients:

$$C_k = \frac{1}{4\pi}\int_{S_{1234}}\frac{\partial}{\partial n}\left(\frac{1}{r_k}\right)dS_k \ ; \quad (8)$$

$$B_k = -\frac{1}{4\pi}\int_{S_{1234}}\frac{1}{r_k}dS_k \ ; \quad (9)$$

where

N - number of panels over the whole aircraft;
N_w - number of panels over the wake;
S_{1234} - area of k-th panel.

For easier paneling the airplane has been divided into a number of segments. Each segment has been divided next into panels as follows:

main wing - 400
pylon - 40
fuselage - 432
tailplane - 200
container - 208.

For the case of symmetric flow 640 panels were used, for the case of asymmetric (arbitrary) flow the full number of panels (1280) was used. Fig.5 shows the whole surface of airplane divided into panels. Fig.6 shows details of paneling in the region of the connection of fuselage, pylon, container and wing. The condition of node compatibility along the adjacent edges has to be fulfilled [10]. It enables moving from one object (segment) to another when differentiating. Moreover, in the discontinuity region, some panel strips on the extreme edge are usually added. This way, dividing into panels in the direction perpendicular to the edge, is compressed. It results in a much smaller interpolation error appearing in the discontinuity region [10].

Wakes were assumed to exist behind main wing and tailplane only. To avoid the iterative process (necessary if the shape of wake should

be determined) it was assumed that wakes are flat. In such a case no boundary condition was imposed over the wake. To obtain the singularities strengths over the wakes it was assumed that these strengths were related to those of distributed on body surface by means of Kutta-Joukowski condition. It enables reduction of number of unknown parameters and equations to the number of panels on the airplane surface. Selected computational results are presented in Fig.7 and include pressure distribution over airplane surface at angle of attack: $\alpha = 4^o$.

Results obtained from panel method, compared and supplemented by DATCOM [2] & ESDU [3] were used in stability analysis. The most important aerodynamic data are summarised below:

- lift curve-slope $C_{L\alpha} = 0.114$ 1/deg
- maximum lift coefficient $C_{Lmax} = 1.2$
- zero lift angle $\alpha_0 = -4.5^o$
- drag polar equation
  $C_D = C_{Dmin} + K * (C_L - C_{L0})^2$ where $K=0.0155$; $C_{L0} = -0.0054$ and C_{Dmin} is given in Tab.2.

Tab.2 Minimum drag coefficient versus flight altitude

H (km)	C_{Dmin}
0	0.013
5	0.013
10	0.013
15	0.015
20	0.022
25	0.042

- pitching moment coefficient (without tailplane) about quarter chord point:

$C_{m,W+B} = -0.008*C_L - 0.10$

- tailplane data: $a_1 = 0.069$ 1/deg ; $a_2 = 0.027$ 1/deg ; $a_{v1} = -.040$; $a_{v2} = 0.016$ 1/deg
- variation of airplane rolling moment coefficient with aileron deflection angle:

$C_{l\delta a} = -0.0027$ 1/deg

- downwash fuction: $\varepsilon = d\varepsilon/d\alpha*\alpha + \varepsilon_0$ ($\alpha=0$), where $d\varepsilon/d\alpha = 0.426$; ε_0 ($\alpha=0$) $= 1.9^o$
- neutral point of stability is placed at 59 % of MAC.

5 Steady trimmed flight conditions

In the steady trimmed flight a number of independent variables has been selected and found from a nonlinear set of equations of equilibrium. Among these independent variables are: thrust, angle of attack and elevator deflection. All these variables are shown versus speed for different flight altitude at Fig.8,9,10. An average gradient of angle of attack and elevator deflection versus speed is practically independent of flight altitude. Gradient of thrust-required curve versus velocity decreases for higher flight altitude, mainly due to increasing the minimum drag coefficient C_{D0} and induced drag coefficient, $K*C_L^2$. Fig.11,12 show lift coefficient on the main wing, and angle of attack, both versus speed for different flight altitude.

6 Dynamic stability

Differential equations of motion together with kinamatic relationship have the form [10,11,12]

$$\mathbf{M}\,\dot{\mathbf{x}} = \mathbf{B}\,\mathbf{x}\,, \qquad (10)$$

where **M** and **B** denote mass and generalized stiffness matrices of order 8x8.

The eigenvalues corresponding to matrix equation are

$$\lambda_i = \xi_i + i*\eta_i\,, \qquad (11)$$

where ξ_i , η_i are damping and frequency coefficients.

Tab.3 Comparison of selected stability derivatives

Dimensionless stability derivatives	STB	Panel method
$x_u = -2C_D - \frac{\partial C_D}{\partial (u/V)}$	-0.052	
$x_w = -\frac{\partial C_D}{\partial (w/V)}$	-0.17	

$x_q = -\frac{\partial C_D}{\partial (qc/V)}$	0.014	
$z_u = -2C_L - \frac{\partial C_L}{\partial (u/V)}$	-1.75	
$z_w = -\frac{\partial C_L}{\partial (w/V)}$	-6.49	-6.2
$z_q = -\frac{\partial C_L}{\partial (qc/V)}$	-2.18	-5.41
$z_{\dot{w}} = -\frac{\partial C_L}{\partial (\dot{w}c/V^2)}$	-0.93	
$m_u = \frac{\partial C_m}{\partial (u/V)}$	-0.11	
$m_w = \frac{\partial C_m}{\partial (w/V)}$	-1.25	-1.2
$m_q = \frac{\partial C_m}{\partial (qc/V)}$	-7.58	-9.65
$m_{\dot{w}} = \frac{\partial C_m}{\partial (\dot{w}c/V^2)}$	-3.13	
$y_v = \frac{\partial C_y}{\partial (v/V)}$	-0.76	-0.59
$y_p = \frac{\partial C_y}{\partial (pb/V)}$	0.12	0.10
$y_r = \frac{\partial C_y}{\partial (rb/V)}$	-0.38	0.027
$l_v = \frac{\partial C_l}{\partial (v/V)}$	0.16	0.026
$l_p = \frac{\partial C_l}{\partial (pb/V)}$	-0.82	-0.37
$l_r = \frac{\partial C_l}{\partial (rb/V)}$	0.19	0.11
$n_v = \frac{\partial C_n}{\partial (v/V)}$	0.14	0.0064
$n_p = \frac{\partial C_n}{\partial (pb/V)}$	0.055	-0.046
$n_r = \frac{\partial C_n}{\partial (rb/V)}$	.0004	-0.0096

The analysis of damping and frequency for natural modes of vibration made with the aid of STB package [13], using different sets of stability derivatives (given in Tab.3) shows that stability characteristics are consistent in quality, and that the existing discrepancies have only a quantitative character. In all cases one does not observe the change of stability type, i.e. changing either from stable state into unstable one or vice versa. Scatter of results (ξ and η) obtained from different models for all modes are rather insignificant. Damping and frequency coefficients for natural modes of vibration are shown in Fig.13-17. Analysis shows that dynamic stability of HARVE-2 deteriorates if the flight altitude increases. Damping of short period, Duch roll, rolling mode and phugoid decreases for higher flight altitude. Spiral is the only one mode, the negative damping (positive ξ) of that decreases for higher flight altitudes. In Tab.4 time to double amplitude for different flight altitude is shown. The short period frequency coefficient (Fig.14) initially increases and then decreases as the flight altitude increases. The Duch Roll frequency coefficient decreases monotonically as the flight altitude increases, Fig.17. Time to double of the spiral mode versus flight altitude is given in Tab.4 and is acceptable in spite of the spiral instability.

Tab.4 Time to double of the spiral mode

H (km)	0	5	10	15	20	25
T_2 (sec)	9	13	15	29	30	44

Fig.18-22 present an influence of airplane mass onto damping and frequency coefficients. One can observe that short period, Dutch roll, phugoid and spiral modes are better damped for smaller mass of airplane. Only the rolling mode damping is weaker for smaller mass. Frequency coefficients of Duch roll and phugoid modes increase for smaller mass, whereas they decrease for the short period mode.

7 Conclusion

Presented analysis can be treated as a starting point for further improvement of dynamic characteristics in the context of flying and handling qualities. Steady trimmed flight

conditions and stability characteristics appeared to be sensitive with respect to a number of aerodynamic characteristics, especially to polar drag curve, downwash and pitching moment coefficient. These characteristics should be computed more accurately in the future analysis, using more advanced CFD methods. Damping of short period and Dutch roll modes for the considered airplane configuration should be augmented using Automatic Flight Control Systems.

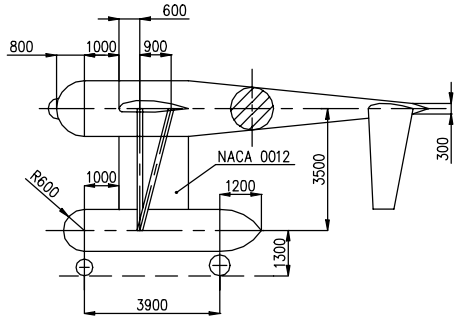

Fig.2 Side view of Harve 2 airplane

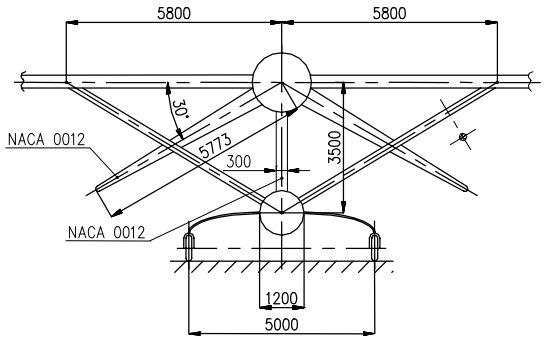

Fig.3 Front view of Harve 2 airplane

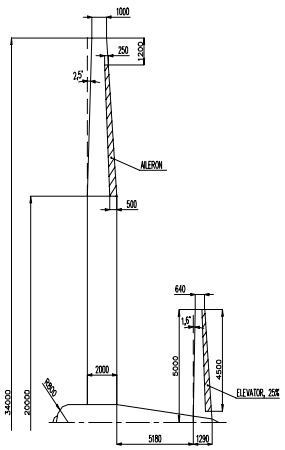

Fig.4 Plain view of whole airplane

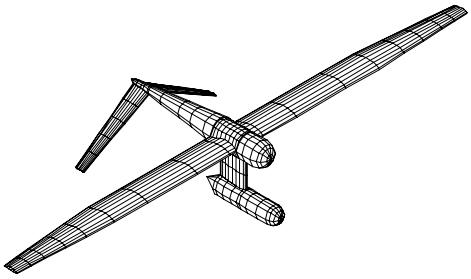

Fig.5 Surface divided into panels

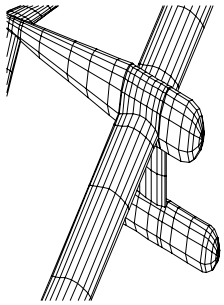

Fig.6 Connection of wing with fuselage and container with pylon

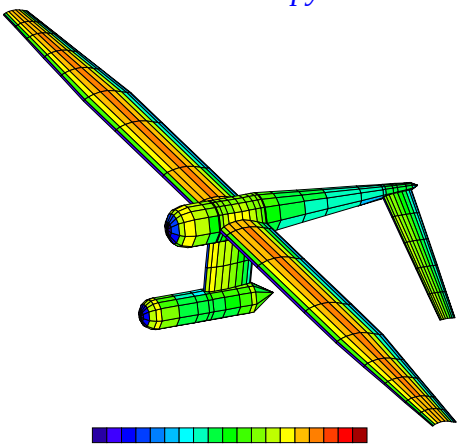

Fig.7 Pressure distribution for $\alpha = 4^o$

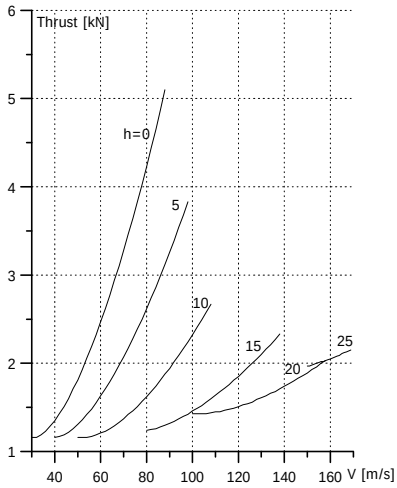

Fig.8 Thrust-required versus speed for various flight altitude

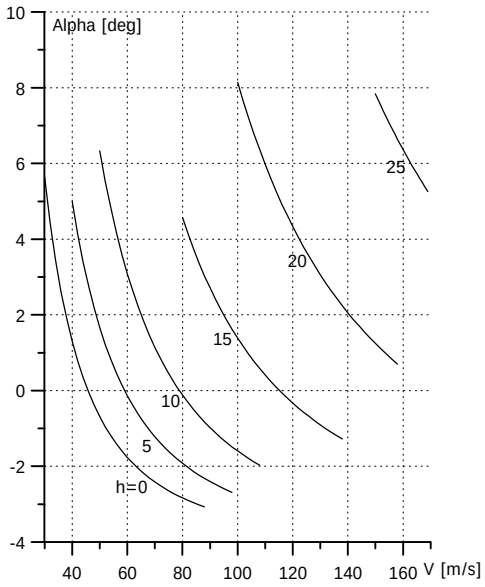

Fig.9 Angle of attack versus speed for various flight altitude

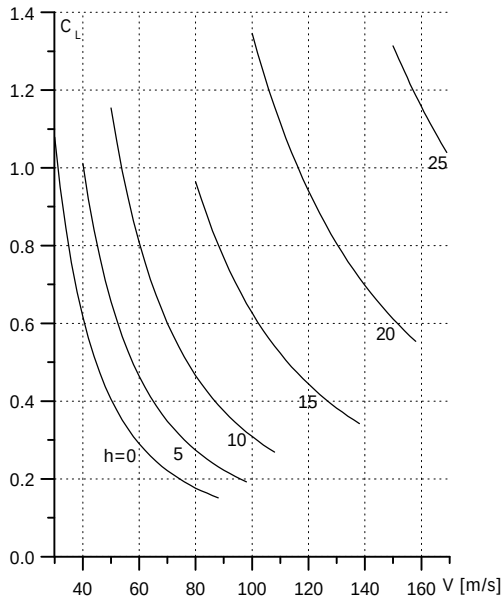

Fig.11 Lift coefficient versus speed for various flight altitude

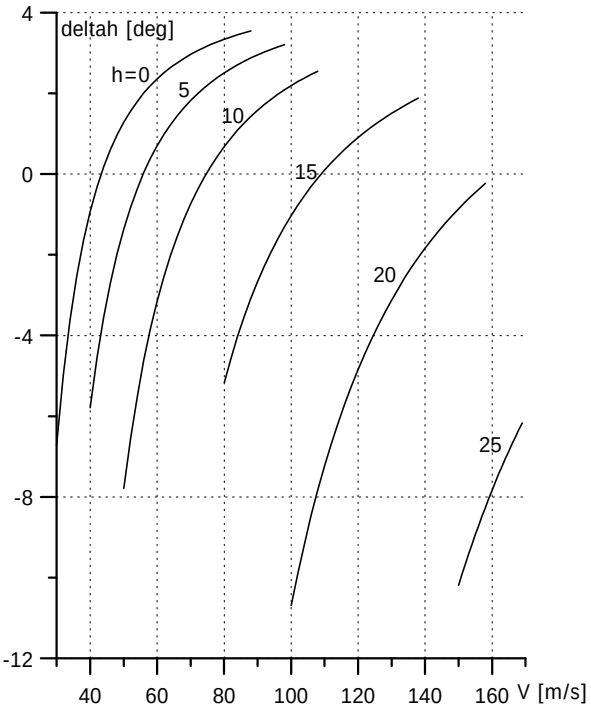

Fig.10 Elevator deflection versus speed for various flight altitude

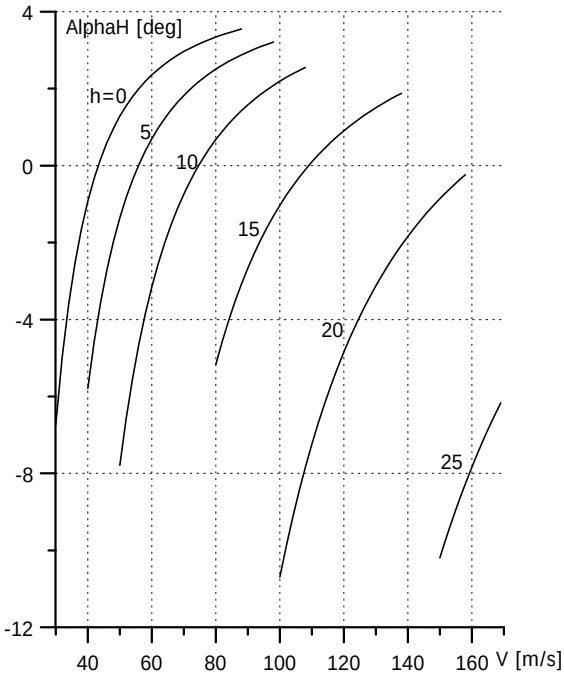

Fig.12 Tailplane angle of attack versus speed for various flight altitude

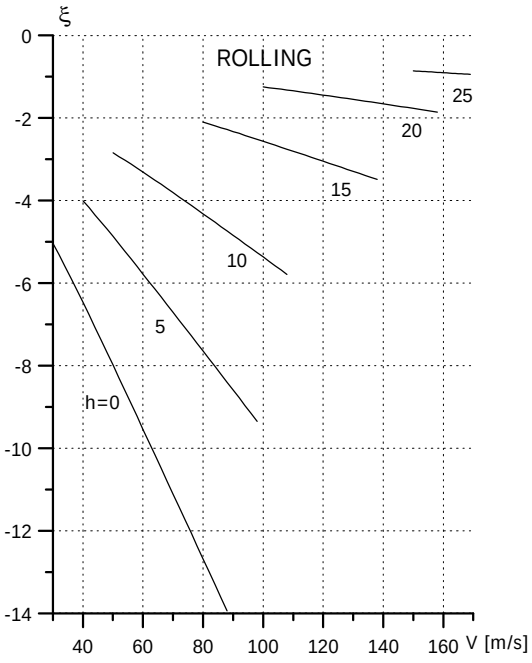

Fig.13 Damping coefficients of rolling mode versus speed for various flight altitude

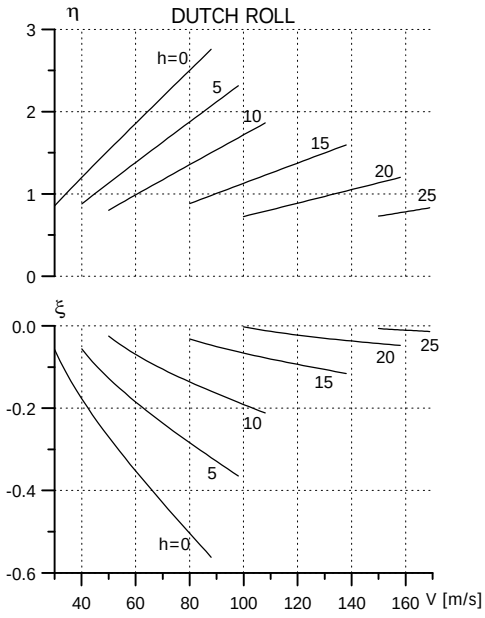

Fig.15 Damping & frequency coefficients of Dutch roll mode versus speed for various flight altitude

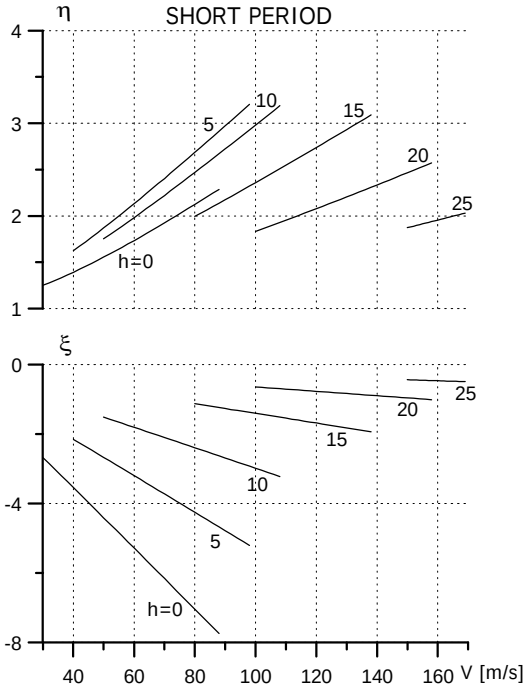

Fig.14 Damping & frequency coefficients of short period mode versus speed for various flight altitude

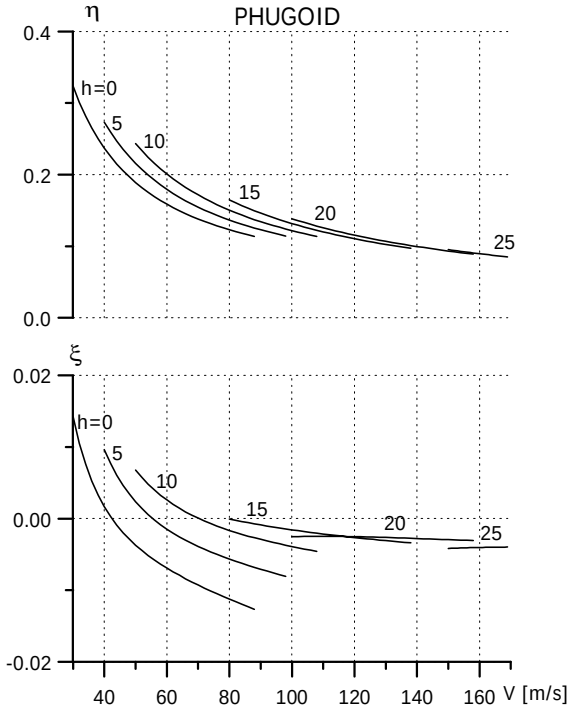

Fig.16 Damping & frequency coefficients of phugoid mode versus speed for various flight altitude

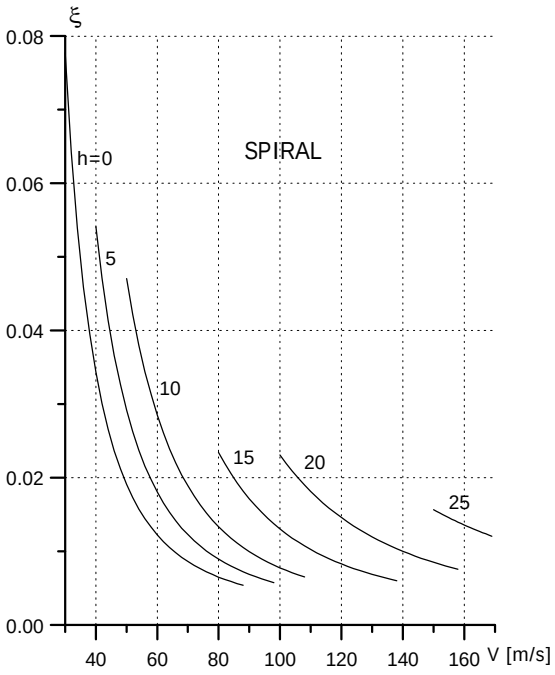

Fig.17 Damping coefficients of spiral mode versus speed for various flight altitude

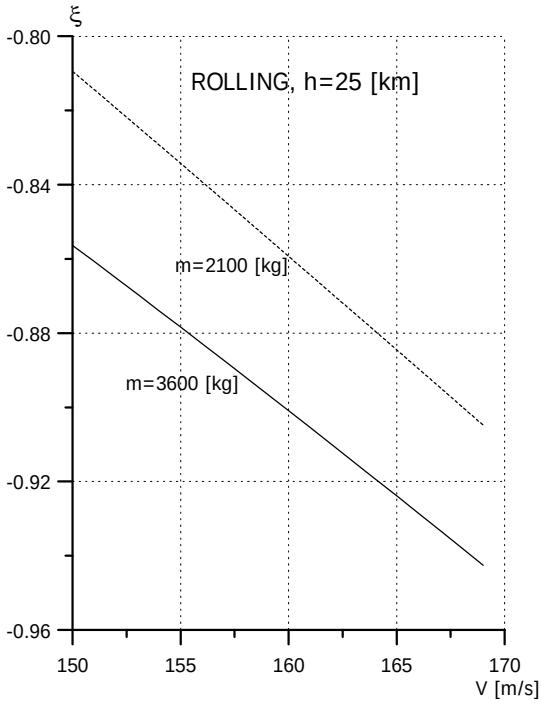

Fig.18 Comparison of damping coefficients of rolling mode versus speed for various mass

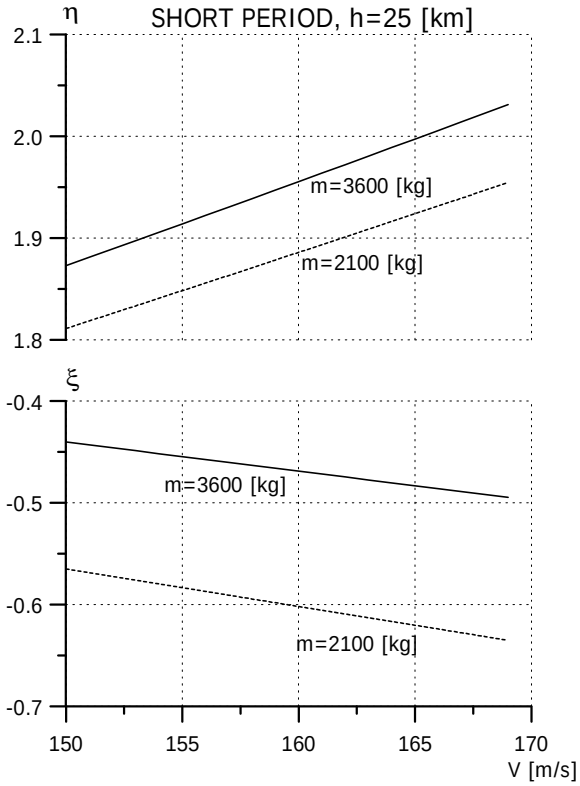

Fig.19 Comparison of damping & frequency coefficients of short period mode versus speed for various mass

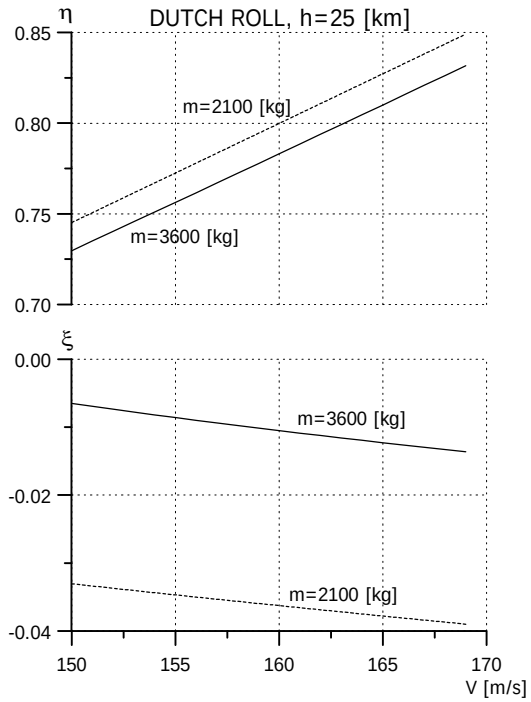

Fig.20 Comparison of damping & frequency coefficients of Duch roll mode versus speed for various mass

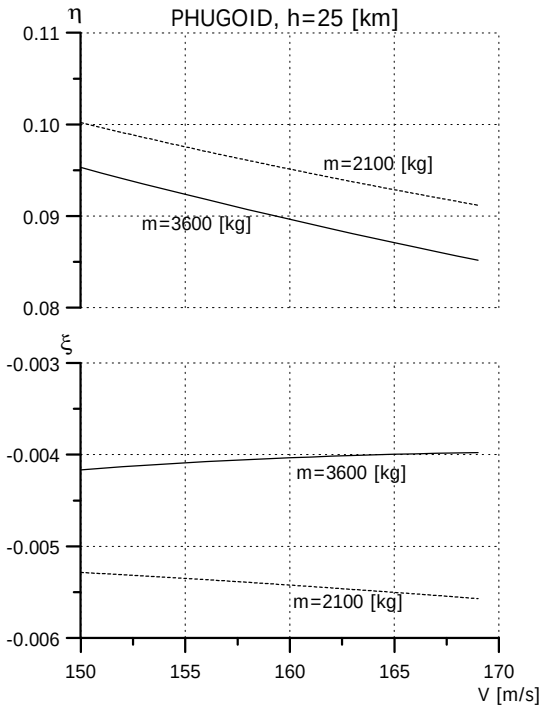

Fig.21 Comparison of damping & frequency coefficients of phugoid mode versus speed for various mass

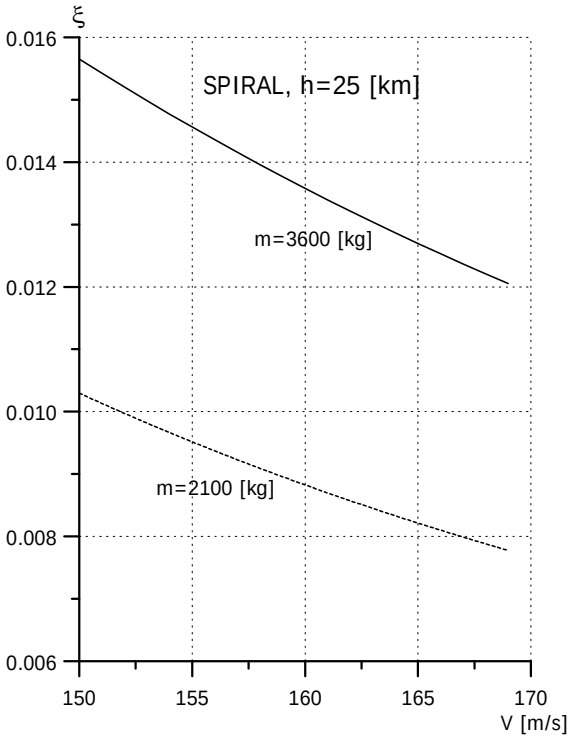

Fig.22Comparison of damping coefficients of spiral mode versus speed for various mass

References

[1] Goraj Z., Frydrychewicz A., Winiecki J. Design concept of a high altitude long endurance unmanned aerial vehicle. *Aircraft Design*, Vol.2 No.1, pp 19-44, 1999.

[2] Fink, R.D. *USAF stability and control DATCOM*. Wright-Patterson AFB, OH, 1975.

[3] Engineering Sciences Data Unit, Sub-series Aerodynamics, 3A, Regent Street, London W1R 7AD, England (ESDU - Data Sheets).

[4] Wortman, A., Wyszkowski, C., Frydrychiewicz, A. and Goraj, Z. High altitude reconnaissance vehicle enterprise. *Design Conceptual Project submitted in DARPA*, Santa Monica, 1995, unpublished.

[5] Bednarek, K., Danilecki, S., Frydychewicz, A., Goraj, Z., et.al. *Conceptual design of high altitude reconnaissance unmanned aerial vehicle - HARVE*. Warsaw University of Technology, Institute of Aeronautics and Applied .Mechanics. Warsaw, 1995, unpublished.

[6] The Strato 2C Project. Grob Luft- und Raumfahrt GMBH & CO.KG. *Company Report*, unpublished, 1995.

[7] Goraj Z., Ueda T. Ultra light wing structure for high altitude long endurance UAV. *ICAS Congress 2000, Harrogate, England. Paper 0476, pp.1-10, 2000.*

[8] Hess J. L., Smith A. M. O. Calculation of potential flow about arbitrary bodies, *Progress in Aeronautical Sciences*, Vol.8, (Ed. D.Küchemann), Pergamon Press, Oxford, pp.1-138, 1967.

[9] Katz J., Plotkin A. Low-speed aerodynamics - from wing theory to panel methods. McGraw-Hill, Inc., New York 1991.

[10] Goraj Z., Kulicki P., Lasek M. Aircraft stability analysis for strongly coupled aerodynamic configuration. *Journal of Theretica & Applied Mechanics.* Vol.35, 1, pp.137-158, 1997.*l*

[11] Cook M.V. *Flight dynamics principles.* 1st edition, Arnold, 1997.

[12] Roskam J. Airplane flight dynamics and automatic flight controls. 1st edition, DARcorporation, 1995.

[13] Goraj Z. *STB-9702 - software for flight dynamics stability analysis.* Numerical package developed in Warsaw University of Technology. Warsaw, 1997.